Optical and Quantum Electronics (2018) 50:432
https://doi.org/10.1007/s11082-018-1685-8

# Novel analytical model for nano-coupler between metal–insulator–metal plasmonic and dielectric slab waveguides

**Mohammad Bagher Heydari**[1] · **Masoud Asgari**[2] · **Niloofar Jafari**[3]

Received: 29 August 2018 / Accepted: 1 November 2018


**Abstract**
We propose a new analytical model for nano-coupler between metal–insulator–metal (MIM) plasmonic and dielectric slab waveguides. By using the boundary conditions and mode matching technique, the analytical expression for transmission coefficient can be achieved at the plasmonic–dielectric junction. The theoretical results are compared with the simulation results of COMSOL software. A good agreement between the simulation and theoretical results is observed which validates our analytical model. The maximum transmission efficiency of the coupler can be obtained by changing the width of the dielectric ($W_d$) and air ($W_a$) layers. For the nano-coupler with $W_d$ = 300 nm at the wavelength 1.55 μm, the results show that maximum transmission efficiency of 75% can be achieved at the width of 63 nm ($W_a$=63 nm). Our analytical model is accurate and can calculate the modal properties of the proposed coupler.

**Keywords** MIM waveguide · Plasmonic · Dielectric slab waveguide · Analytical model

## 1 Introduction

With the advances of plasmonics in recent years, scientists have interested in designing plasmonic devices due to their unique properties, such as strong confinement at the small scales (Maier 2007). The field confinement opens new aspects in optical communications to miniaturize the photonic integrated circuits. Plasmonic waveguides composed by metal–insulator–metal (MIM) have been reported in numerous articles. These waveguides have various structures such as metallic strips and nanowires (Chu et al. 2008), metallic grooves (Bozhevolnyi et al. 2005), plasmonic slot waveguide (Chen et al. 2006) and plasmonic waveguides (Liu et al. 2005; Kusunoki et al. 2005; Tanaka and Tanaka 2003; Pile

✉ Mohammad Bagher Heydari
mo_heydari@elec.iust.ac.ir

[1] Electrical Engineering Department, Iran University of Science and Technology (IUST), Tehran, Iran

[2] Electrical Engineering Group, Imam Khomeini International University (IKIU), Qazvin, Iran

[3] Electrical Engineering Group, Payam Noor University, Zanjan, Iran

Published online: 10 November 2018

et al. 2005). However, the plasmonics devices are not limited to plasmonic waveguides. In recent years, a large variety of plasmonic devices are introduced and studied which include filters (Mei et al. 2010), absorption switches (Min and Veronis 2009), couplers (Rezaei et al. 2012), resonators (Diest et al. 2009) and power splitters (Reiserer et al. 2010).

One of the interesting plasmonic structures is Nano-couplers which connect the dielectric waveguides to plasmonic devices. This coupler is designed to decrease the propagation losses due to metallic interaction. Several methods have been presented to achieve this purpose like direct coupling (Veronis and Fan 2007), adiabatic and non-adiabatic tapered couplers (Pile and Gramotnev 2006; Ginzburg et al. 2006), $\lambda/4$ coupler (Ginzburg and Orenstein 2007) and multi-section taper (Veronis and Fan 2007).

The specific case of direct coupling between MIM and dielectric slab waveguides has been investigated in many articles. The first study on the modal properties for compact couplers of the dielectric slab and MIM plasmonic waveguides was done in Veronis and Fan (2007). They reported 70% transmission efficiency at the optical communication wavelength for the proposed coupler. Also, the authors introduced a coupler consisting of multi-section taper in this paper (Veronis and Fan 2007). Novel compact couplers and splitters based on Veronis and Fan (2007) were investigated in Wahsheh et al. (2009). In this work, the authors showed that nano-scale plasmonic splitters could be designed with a coupling efficiency of 45% for each branch at telecommunication wavelength. A plasmonic interconnector based on an asymmetric junction between MIM and dielectric slab waveguide with approach 88.5% efficiency was proposed and studied in Lee et al. (2011). In Mote et al. (2012), an efficient coupler is introduced to the interface hybrid dielectric-loaded plasmonic waveguide with Si slab waveguide which can be utilized in on-chip hybrid integrated circuits. An experimental realization of a compact coupler was reported in Emboras et al. (2012). In this research, the coupler was fabricated by CMOS technology processes. Analyzing the plasmonic-dielectric coupler by the circuit model was done in Hodaei et al. (2013). They utilized a stub in Nano coupler to enhance the efficiency of the coupler. In 2013, a coupler was considered at optical communication frequency which was composed by a PEC periodic corrugated metallic parallel plate waveguide and a silicon micro slab (Liu et al. 2013). The coupling efficiency of 98% has been achieved for 300 nm gap size (Liu et al. 2013). In Lima et al. (2017), a directional coupler has been investigated with an efficient power conversion.

In this paper, an accurate model for MIM-slab dielectric coupler will be derived. We apply mode-matching technique to match the electromagnetic fields in MIM and dielectric slab waveguide by using boundary conditions at plasmonic–dielectric borders which the most energies have been concentrated. The paper is organized as follows. In Sect. 2, a semi-analytical model will be presented to describe the modal properties of the coupler. This section starts with Maxwell equations to derive the model. Then, simulation results have been compared with analytical results in Sect. 3. To investigate the effect of dielectric width ($W_d$) and air width ($W_a$) on the transmission spectrum, a parametric study has been done in this section. Finally, Sect. 4 concludes the paper.

## 2 Analytical model

Figure 1 represents the structure of nano-coupler between MIM plasmonic waveguide and the dielectric slab waveguide. The air gap (with a width of $W_a$) is sandwiched between two metal (with permittivity of $\varepsilon_m$) layers in symmetric MIM plasmonic waveguide. In the dielectric

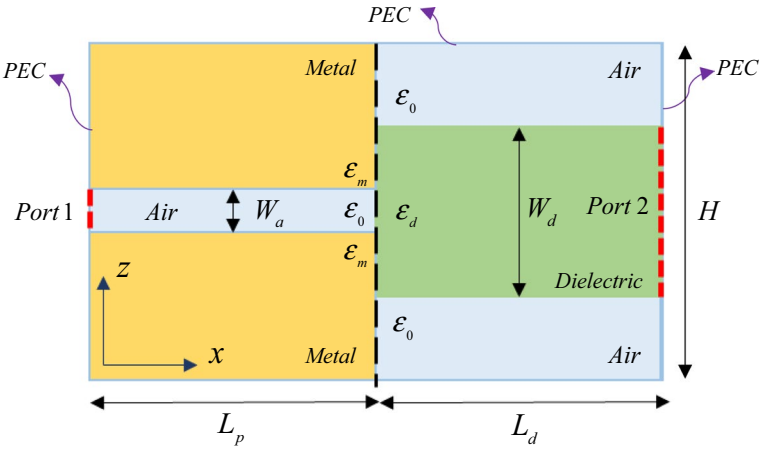


**Fig. 1** The proposed nano-coupler between MIM plasmonic waveguide and the dielectric slab waveguide

slab waveguide, the dielectric layer with permittivity of $\varepsilon_d$ and width of $W_d$ has been placed between two air layers. The incident wave can be propagated initially from either port 1 or port 2. The surrounding of the whole structure is assumed to be Perfect Electric Conductor (PEC) which has no plasmonic feature in simulations. It should be noted that we bounded the structure to PEC because the coupler has finite and bounded dimensions in the practical applications.

Let us suppose that both waveguides propagate TM mode, and the electromagnetic fields are independent of $y$ ($\partial/\partial y = 0$). Therefore, from Maxwell equations (Pozar 2009):

$$\frac{\partial^2 H_y}{\partial z^2} + \left(k_0^2 \varepsilon - \beta^2\right) H_y = 0 \tag{1}$$

where $k_0$ and $\beta$ are the wave number of the air and propagation constant, respectively.

Transverse components can be written as (Pozar 2009):

$$\begin{cases} E_x = \dfrac{1}{i\omega\varepsilon_0\varepsilon} \dfrac{\partial H_y}{\partial z} \\ E_z = \dfrac{-1}{i\omega\varepsilon_0\varepsilon} \dfrac{\partial H_y}{\partial x} \end{cases} \tag{2}$$

In the MIM plasmonic waveguide, one can write:

$$H_y(x,z) = \begin{cases} A_1^+ e^{i\beta x} e^{k_1 z} + A_1^- e^{-i\beta x} e^{k_1 z} + A_2^+ e^{i\beta x} e^{-k_1 z} + A_2^- e^{-i\beta x} e^{-k_1 z} & |z| \le W_a/2 \\ A_3^+ e^{i\beta x} e^{k_2 z} + A_3^- e^{-i\beta x} e^{k_2 z} & z \le -W_a/2 \\ A_4^+ e^{i\beta x} e^{-k_2 z} + A_4^- e^{-i\beta x} e^{-k_2 z} & z \ge W_a/2 \end{cases} \tag{3}$$

As mentioned before, the MIM structure is symmetric and,

$$\begin{cases} k_0^2 - \beta^2 = -k_1^2 \\ k_0^2 \varepsilon_m - \beta^2 = -k_2^2 \end{cases} \tag{4}$$

It should be noted that the permittivity of metal ($\varepsilon_m$) is described by Drude's Model (Han et al. 2007):

$$\varepsilon_m = \varepsilon_\infty - \frac{\omega_p^2}{\omega(\omega - j\gamma)} \tag{5}$$

In the above equation,$\omega_p$, $\gamma$ and $\varepsilon_\infty$ are the plasma frequency, the collision rate and the permittivity of the metal at large frequencies, respectively. Now, the transverse fields can be calculated for various regions of the MIM plasmonic structure by substituting (3) to (2). In the dielectric waveguide, the magnetic fields are expressed as:

$$H_y(x,z) = \begin{cases} B_1^+ e^{i\beta x}\sin(k_3 z) + B_1^- e^{-i\beta x}\sin(k_3 z) + B_2^+ e^{i\beta x}\cos(k_3 z) + B_2^- e^{-i\beta x}\cos(k_3 z) & |z| \le W_d/2 \\ B_3^+ e^{i\beta x} e^{k_1 z} + B_3^- e^{-i\beta x} e^{k_1 z} & z \le -W_d/2 \\ B_4^+ e^{i\beta x} e^{-k_1 z} + B_4^- e^{-i\beta x} e^{-k_1 z} & z \ge W_d/2 \end{cases} \tag{6}$$

where

$$k_0^2 \varepsilon_d - \beta^2 = k_3^2 \tag{7}$$

By substituting the (6) to (2), the transverse fields can be achieved for various regions of the dielectric slab waveguide. Let us suppose that the coupler is excited from Port 1 (Port 2 is off). As the incident waves reach to the plasmonic-dielectric junction (at $x = L_p$), some of them reflect back in MIM waveguide (as denoted by $A_1^-$ , $A_2^-$ , $A_3^-$ , $A_4^-$ coefficients) and the transmitted waves are generated in all regions of the dielectric slab waveguide. If the structure is unbounded, these transmitted waves only will exist in the dielectric slab structure. However, the coupler is not unbounded and has a certain length ($L_d$) in the practical applications. By simulating the structure in the software, the surrounding borders are supposed PEC with no plasmonic properties. Therefore, when the transmitted waves reach to the right borders, the reflected waves are produced in the various regions of the dielectric slab waveguide, as illustrated in Fig. 2. These reflected waves in this waveguide are denoted by $B_1^-$ , $B_2^-$ , $B_3^-$ , $B_4^-$ coefficients.

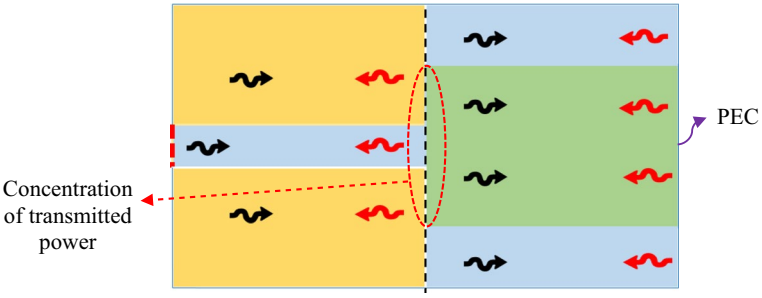


**Fig. 2** Transmitted and reflected waves in various regions of MIM plasmonic waveguide and dielectric slab waveguide (port 2 is off). The black and red allows represent the transmitted and reflected waves, respectively. (Color figure online)

Now, the boundary conditions should be applied to calculate the transmission coefficient of the coupler. It must be emphasized that the full analysis of the proposed coupler is so complicated, but we utilize the boundary conditions just for the inner boundaries in the plasmonic-dielectric junction due to the concentration of the most energy in these borders. By this method, the fields will be matched properly. For port 1 at $x = 0$, one can write:

$$E_z\,|_{x=0\ \left(|z|\le\frac{W_a}{2}\right)} = E_0 \tag{8}$$

Which leads to

$$A_1^+ - A_1^- + A_2^+ - A_2^- = \frac{-\omega\varepsilon_0 k_1}{2\beta\sinh\left(\frac{k_1 W_a}{2}\right)}E_0 \tag{9}$$

In (9), $E_0$ is the amplitude of the incident wave in the z-direction at port 1. Similarly, for port 2 at $x = L_p + L_d$ (port 2 is supposed to be off and PEC here),

$$E_z\,|_{x=L_p+L_d\ \left(|z|\le\frac{W_d}{2}\right)} = 0 \tag{10}$$

Which results in

$$B_2^+ e^{i\beta(L_p+L_d)} - B_2^- e^{-i\beta(L_p+L_d)} = 0 \tag{11}$$

It should be noted that we have integrated over $(-W_a/2,\ W_a/2)$ in (10) to derive an equation independent of z. Boundary conditions at $z = W_a/2, -W_a/2$ in the MIM plasmonic waveguide are expressed as:

$$H_{y1} = H_{y2}\,|_{z=\frac{W_a}{2}\ (0\le x\le L_p)}\ ,\ E_{x1} = E_{x2}\,|_{z=\frac{W_a}{2}\ (0\le x\le L_p)} \tag{12}$$

$$H_{y1} = H_{y2}\,|_{z=-\frac{W_a}{2}\ (0\le x\le L_p)}\ ,\ E_{x1} = E_{x2}\,|_{z=-\frac{W_a}{2}\ (0\le x\le L_p)} \tag{13}$$

By integrating over $(0,\ L_p)$ for (12), one can obtain:

$$\left(e^{j\beta L_p}-1\right)\left[A_1^+ e^{\frac{k_1 W_a}{2}} + A_2^+ e^{-\frac{k_1 W_a}{2}} - A_4^+ e^{-\frac{k_2 W_a}{2}}\right] + \left(1-e^{-j\beta L_p}\right)\left[A_1^- e^{\frac{k_1 W_a}{2}} + A_2^- e^{-\frac{k_1 W_a}{2}} - A_4^- e^{-\frac{k_2 W_a}{2}}\right] = 0 \tag{14}$$

$$\begin{aligned}&\left(e^{j\beta L_p}-1\right)\left[A_1^+ e^{\frac{k_1 W_a}{2}} - A_2^+ e^{-\frac{k_1 W_a}{2}} + \frac{k_2}{k_1\varepsilon_m}A_4^+ e^{-\frac{k_2 W_a}{2}}\right]\\ &+\left(1-e^{-j\beta L_p}\right)\left[A_1^- e^{\frac{k_1 W_a}{2}} - A_2^- e^{-\frac{k_1 W_a}{2}} + \frac{k_2}{k_1\varepsilon_m}A_4^- e^{-\frac{k_2 W_a}{2}}\right] = 0\end{aligned} \tag{15}$$

From (13),

$$\left(e^{j\beta L_p}-1\right)\left[A_1^+ e^{-\frac{k_1 W_a}{2}} + A_2^+ e^{\frac{k_1 W_a}{2}} - A_3^+ e^{-\frac{k_2 W_a}{2}}\right] + \left(1-e^{-j\beta L_p}\right)\left[A_1^- e^{-\frac{k_1 W_a}{2}} + A_2^- e^{\frac{k_1 W_a}{2}} - A_3^- e^{-\frac{k_2 W_a}{2}}\right] = 0 \tag{16}$$

$$\left(e^{j\beta L_p}-1\right)\left[A_1^+e^{-\frac{k_1W_a}{2}}-A_2^+e^{\frac{k_1W_a}{2}}-\frac{k_2}{k_1\varepsilon_m}A_3^+e^{-\frac{k_2W_a}{2}}\right]+\left(1-e^{-j\beta L_p}\right)\left[A_1^-e^{-\frac{k_1W_a}{2}}-A_2^-e^{\frac{k_1W_a}{2}}-\frac{k_2}{k_1\varepsilon_m}A_3^-e^{-\frac{k_2W_a}{2}}\right]=0 \tag{17}$$

In the dielectric slab waveguide, similar boundary conditions can be written at $z = W_d/2, -W_d/2$ and then integrate over $(L_p, L_p + L_d)$ to achieve the following relations:

$$e^{j\beta L_p}\left(e^{j\beta L_d}-1\right)\left[B_1^+\sin\left(\frac{k_3W_d}{2}\right)+B_2^+\cos\left(\frac{k_3W_d}{2}\right)-B_4^+e^{-\frac{k_1W_d}{2}}\right]+e^{-j\beta L_p}\left(1-e^{-j\beta L_d}\right)\left[B_1^-\sin\left(\frac{k_3W_d}{2}\right)+B_2^-\cos\left(\frac{k_3W_d}{2}\right)-B_4^-e^{-\frac{k_1W_d}{2}}\right]=0 \tag{18}$$

$$e^{j\beta L_p}\left(e^{j\beta L_d}-1\right)\left[B_1^+\cos\left(\frac{k_3W_d}{2}\right)+B_2^+\sin\left(\frac{k_3W_d}{2}\right)+\frac{k_1\varepsilon_3}{k_3}B_4^+e^{-\frac{k_1W_d}{2}}\right]+e^{-j\beta L_p}\left(1-e^{-j\beta L_d}\right)\times\left[B_1^-e^{-\frac{j\beta(L_p+L_d)}{2}}\cos\left(\frac{k_3W_d}{2}\right)-B_2^-e^{-\frac{j\beta(L_p+L_d)}{2}}\sin\left(\frac{k_3W_d}{2}\right)+\frac{k_1\varepsilon_3}{k_3}B_4^-e^{-\frac{k_1W_d}{2}}\right]=0 \tag{19}$$

$$e^{j\beta L_p}\left(e^{j\beta L_d}-1\right)\left[-B_1^+\sin\left(\frac{k_3W_d}{2}\right)+B_2^+\cos\left(\frac{k_3W_d}{2}\right)-B_3^+e^{-\frac{k_1W_d}{2}}\right]+e^{-j\beta L_p}\left(1-e^{-j\beta L_d}\right)\left[-B_1^-\sin\left(\frac{k_3W_d}{2}\right)+B_2^-\cos\left(\frac{k_3W_d}{2}\right)-B_3^-e^{-\frac{k_1W_d}{2}}\right]=0 \tag{20}$$

$$e^{j\beta L_p}\left(e^{j\beta L_d}-1\right)\left[B_1^+\cos\left(\frac{k_3W_d}{2}\right)+B_2^+\sin\left(\frac{k_3W_d}{2}\right)-\frac{k_1\varepsilon_3}{k_3}B_3^+e^{-\frac{k_1W_d}{2}}\right]+e^{-j\beta L_p}\left(1-e^{-j\beta L_d}\right)\left[B_1^-\cos\left(\frac{k_3W_d}{2}\right)+B_2^-\sin\left(\frac{k_3W_d}{2}\right)-\frac{k_1\varepsilon_3}{k_3}B_3^-e^{-\frac{k_1W_d}{2}}\right]=0 \tag{21}$$

Now, we should use boundary conditions at the plasmonic–dielectric junction of MIM waveguide and slab dielectric waveguide (at $x = L_p$). As mentioned before, most of the transmitted power is concentrated in the middle of two waveguides (see Fig. 2). Therefore, the boundary conditions have been applied just for the inner boundaries of the common border between two waveguides. Boundary conditions at $x = L_p$ are:

$$H_{y1}=H_{y2}\big|_{x=L_p\left(|z|\le\frac{W_a}{2}\right)},\quad E_{z1}=E_{z2}\big|_{x=L_p\left(|z|\le\frac{W_a}{2}\right)} \tag{22}$$

$$H_{y1}=H_{y2}\big|_{x=L_p\left(\frac{W_a}{2}\le z\le\frac{W_d}{2}\right)},\quad E_{z1}=E_{z2}\big|_{x=L_p\left(\frac{W_a}{2}\le z\le\frac{W_d}{2}\right)} \tag{23}$$

$$H_{y1}=H_{y2}\big|_{x=L_p\left(-\frac{W_d}{2}\le z\le-\frac{W_a}{2}\right)},\quad E_{z1}=E_{z2}\big|_{x=L_p\left(-\frac{W_d}{2}\le z\le-\frac{W_a}{2}\right)} \tag{24}$$

From (22), we obtain:

$$\frac{k_3}{k_1}\sinh\left(\frac{k_1 W_a}{2}\right)\left(A_1^+ e^{j\beta L_p}+A_1^- e^{-j\beta L_p}+A_2^+ e^{j\beta L_p}+A_2^- e^{-j\beta L_p}\right)=\sin\left(\frac{k_3 W_a}{2}\right)\left(B_2^+ e^{j\beta L_p}+B_2^- e^{-j\beta L_p}\right) \tag{25}$$

$$\frac{k_3\varepsilon_3}{k_1}\sinh\left(\frac{k_1 W_a}{2}\right)\left(A_1^+ e^{j\beta L_p}-A_1^- e^{-j\beta L_p}+A_2^+ e^{j\beta L_p}-A_2^- e^{-j\beta L_p}\right)=\sin\left(\frac{k_3 W_a}{2}\right)\left(B_2^+ e^{j\beta L_p}-B_2^- e^{-j\beta L_p}\right) \tag{26}$$

From (23),

$$\begin{aligned}&\frac{k_3}{k_2}e^{-k_2\left(\frac{W_d+W_a}{4}\right)}\sinh\left(\frac{k_2(W_d-W_a)}{4}\right)\left(A_4^+ e^{j\beta L_p}+A_4^- e^{-j\beta L_p}\right)\\&=\left(\cos\left(\frac{k_3 W_a}{2}\right)-\cos\left(\frac{k_3 W_d}{2}\right)\right)\left(B_1^+ e^{j\beta L_p}+B_1^- e^{-j\beta L_p}\right)\\&\quad+\left(\sin\left(\frac{k_3 W_d}{2}\right)-\sin\left(\frac{k_3 W_a}{2}\right)\right)\left(B_2^+ e^{j\beta L_p}+B_2^- e^{-j\beta L_p}\right)\end{aligned} \tag{27}$$

$$\begin{aligned}&\frac{k_3\varepsilon_3}{k_2\varepsilon_2}e^{-k_2\left(\frac{W_d+W_a}{4}\right)}\sinh\left(\frac{k_2(W_d-W_a)}{4}\right)\left(A_4^+ e^{j\beta L_p}-A_4^- e^{-j\beta L_p}\right)\\&=\left(\cos\left(\frac{k_3 W_a}{2}\right)-\cos\left(\frac{k_3 W_d}{2}\right)\right)\left(B_1^+ e^{j\beta L_p}-B_1^- e^{-j\beta L_p}\right)\\&\quad+\left(\sin\left(\frac{k_3 W_d}{2}\right)-\sin\left(\frac{k_3 W_a}{2}\right)\right)\left(B_2^+ e^{j\beta L_p}-B_2^- e^{-j\beta L_p}\right)\end{aligned} \tag{28}$$

And from (24),

$$\begin{aligned}&\frac{k_3}{k_2}e^{-k_2\left(\frac{W_d+W_a}{4}\right)}\sinh\left(\frac{k_2(W_d-W_a)}{4}\right)\left(A_3^+ e^{j\beta L_p}+A_3^- e^{-j\beta L_p}\right)\\&=-\left(\cos\left(\frac{k_3 W_a}{2}\right)-\cos\left(\frac{k_3 W_d}{2}\right)\right)\left(B_1^+ e^{j\beta L_p}+B_1^- e^{-j\beta L_p}\right)\\&\quad+\left(\sin\left(\frac{k_3 W_d}{2}\right)-\sin\left(\frac{k_3 W_a}{2}\right)\right)\left(B_2^+ e^{j\beta L_p}+B_2^- e^{-j\beta L_p}\right)\end{aligned} \tag{29}$$

$$\begin{aligned}&\frac{k_3\varepsilon_3}{k_2\varepsilon_2}e^{-k_2\left(\frac{W_d+W_a}{4}\right)}\sinh\left(\frac{k_2(W_d-W_a)}{4}\right)\left(A_3^+ e^{j\beta L_p}-A_3^- e^{-j\beta L_p}\right)\\&=-\left(\cos\left(\frac{k_3 W_a}{2}\right)-\cos\left(\frac{k_3 W_d}{2}\right)\right)\left(B_1^+ e^{j\beta L_p}-B_1^- e^{-j\beta L_p}\right)\\&\quad+\left(\sin\left(\frac{k_3 W_d}{2}\right)-\sin\left(\frac{k_3 W_a}{2}\right)\right)\left(B_2^+ e^{j\beta L_p}-B_2^- e^{-j\beta L_p}\right)\end{aligned} \tag{30}$$

Now, the analytical model is completed for our proposed coupler. Transmission coefficient of the whole structure can be achieved by Tamir (1975):

$$T(\omega)\approx\frac{\int_z E_t(z,\omega)\times H_p^*(z,\omega)dz-\int_z E_p^*(z,\omega)\times H_t(z,\omega)dz}{\int_z E_t(z,\omega)\times H_p^*(z,\omega)dz+\int_z E_p^*(z,\omega)\times H_t(z,\omega)dz} \tag{31}$$

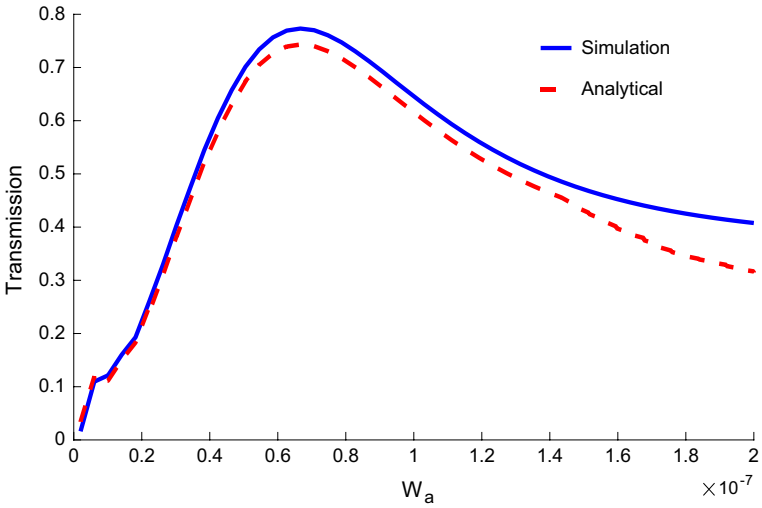


**Fig. 3** Simulation (solid blue line) and analytical (dashed red line) results for the transmission efficiency as a function of air width ($W_a$) for constant dielectric width ($W_d = 300\,\text{nm}$) at the wavelength $\lambda_0 = 1.55\,\mu\text{m}$. Other geometrical parameters are $H = 900\,\text{nm}$, $L_d = L_p = 300\,\text{nm}$. (Color figure online)

where $E_t, H_t$ are transverse electric and magnetic fields at the junction ($x = L_p$) and $E_p, H_p$ are transverse components of electromagnetic fields in MIM plasmonic waveguide (see 2 and 3).

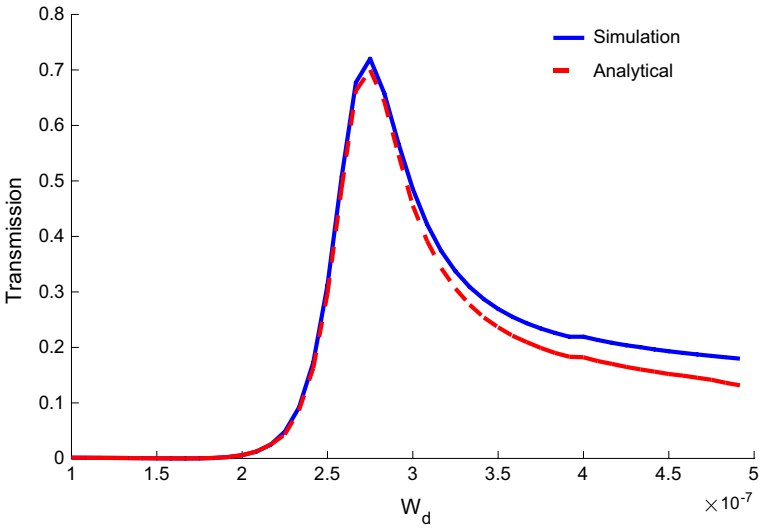


**Fig. 4** Simulation (solid blue line) and analytical (dashed red line) results for the transmission efficiency as a function of dielectric width ($W_d$) for constant air width ($W_a = 60\,\text{nm}$) at the wavelength $\lambda_0 = 1.55\,\mu\text{m}$. Other geometrical parameters are $H = 900\,\text{nm}$, $L_d = L_p = 300\,\text{nm}$. (Color figure online)

## 3 Results and discussion

This section studies the simulation and analytical results more precisely. The air layer has the length of 300 nm ($L_p = 300$ nm) in the MIM plasmonic waveguide. The metal is assumed to be silver, and the parameters of Drude's model are $\omega_p = 1.38 \times 10^{16}$ rad/s, $\gamma = 2.73 \times 10^{13}$ and $\varepsilon_\infty = 3.7$ for it (see Eq. 5). In the dielectric slab waveguide, the dielectric is supposed to be silicon with permittivity of 11.56 and width of 300 nm ($W_d = 300$ nm). Other geometrical parameters are $H = 900\,\text{nm}$, $L_d = 300\,\text{nm}$.

Figure 3 exhibits the transmission efficiency of the coupler as a function of air width ($W_a$) at the wavelength $\lambda_0 = 1.55$ μm. The simulation results are illustrated by a solid blue line, and the dashed red lines show analytical results. As seen in this figure, there is good agreement between the analytical and simulation results. Furthermore, one can observe that the maximum transmission efficiency of 75% occurs at a width of 63 nm ($W_a \approx 63\,\text{nm}$). As emphasized in the previous section, we have neglected the boundary conditions in metal-air boundaries at the common plasmonic–dielectric junction to match the fields successfully, due to the concentration of transmitted power in the middle part of MIM plasmonic and dielectric slab waveguides (see Fig. 2). As the air width of plasmonic waveguide ($W_a$) increases, the power splits into outer areas and the accuracy of our model decreases. Therefore, the disparity between the simulation and analytical results increases as the width of plasmonic layer ($W_a$) increases, as seen in Fig. 3.

To investigate the effect of dielectric width ($W_d$) on the transmission spectrum, it is necessary to depict the transmission efficiency as a function of dielectric width ($W_d$) for constant air width ($W_a = 60\,\text{nm}$). Figure 4 demonstrates the analytical and simulation results for the transmission efficiency as a function of dielectric width ($W_d$) at the wavelength $\lambda_0 = 1.55$ μm. Comparison of solid and dashed curves indicates that the analytical model has acceptable results, especially for $W_d < 320\,\text{nm}$. Furthermore, the structure can be optimized for maximum transmission of 73% at $W_d \approx 280\,\text{nm}$.

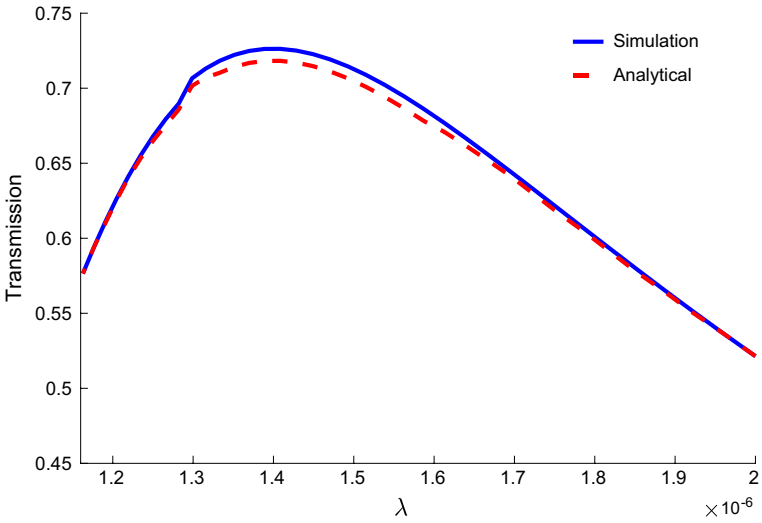


**Fig. 5** The transmission efficiency of the proposed coupler as a function of the wavelength ($\lambda$) for $W_d = 300\,\text{nm}$ and $W_a = 60\,\text{nm}$. Other geometrical parameters are $H = 900\,\text{nm}$, $L_d = L_p = 300\,\text{nm}$

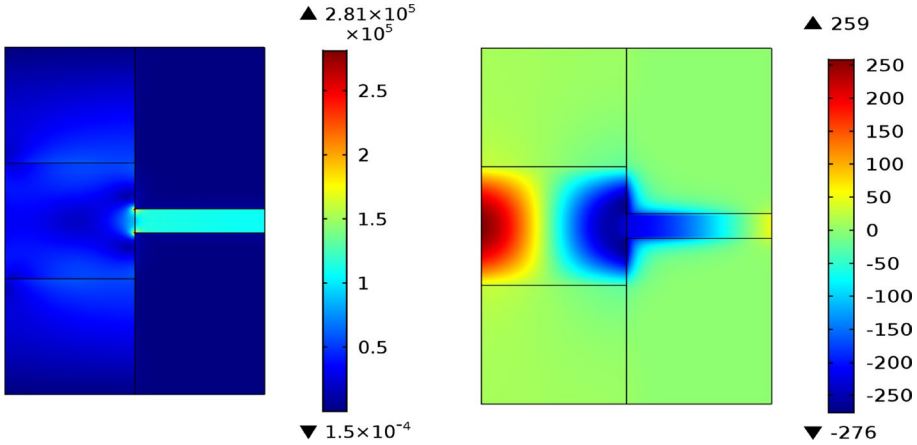


**Fig. 6** Profile of the magnetic field $H_y$ (right picture) and the electric field amplitude $|E|$ (left picture) for $W_d = 320\,\text{nm}$ and $W_a = 65\,\text{nm}$. The coupler has been stimulated from the dielectric slab side (port 2). Other geometrical parameters are $H = 900\,\text{nm}$, $L_d = L_p = 300\,\text{nm}$

In Fig. 5, the transmission efficiency of the proposed coupler has been depicted as a function of the wavelength. Again, the accuracy of our mathematical model is confirmed. It is obvious that the transmission efficiency is close to its optimum amount in a broad range of wavelengths. Also, the maximum transmission occurs near the wavelength of 1.35 μm for this design ($W_d = 300\,\text{nm}$ and $W_a = 60\,\text{nm}$).

As a final point, it must be mentioned that the coupler can be excited from both port 1 or port 2 in our analytical model, as discussed before. This means that our theoretical model can be utilized for the coupler of the dielectric slab to MIM plasmonic waveguide (the structure is excited from port 2 and therefore, the relations (8) and (10) are changed). The profile of magnetic and electric fields for $W_d = 320\,\text{nm}$ and $W_a = 65\,\text{nm}$ are represented in Fig. 6. In this figure, the structure has been stimulated from the dielectric slab side (Port 2). As emphasized before, most of the transmitted power is concentrated in the middle part of MIM plasmonic and dielectric slab waveguides, which Fig. 6 represents this matter.

## 4 Conclusion

In this article, we utilized the mode matching technique to theoretically study the properties of compact couplers between dielectric slab waveguides and two-dimensional MIM plasmonic waveguides. The transmission coefficient was calculated at the plasmonic–dielectric junction in this paper. Then, the structure simulated in COMSOL software and simulation results were compared with analytical results. Our theoretical model was accurate and could estimate the transmission spectrum of the coupler as well. A parametric study was done to study the effects of the dielectric and air gap width on the transmission spectrum. We observed that our analytical model had acceptable results, especially for $W_d < 320\,\text{nm}$, $W_a < 63\,\text{nm}$. For the nano-coupler with $W_d$=300 nm at the wavelength 1.55 μm, the results showed that maximum transmission efficiency of 75% could be obtained at the width of 63 nm ($W_a$=63 nm).

## References


Bozhevolnyi, S.I., Volkov, V.S., Devaux, E., Ebbesen, T.W.: Channel plasmon-polariton guiding by subwavelength metal grooves. Phys. Rev. Lett. **95**(4), 046802 (2005)

Chen, L., Shakya, J., Lipson, M.: Subwavelength confinement in an integrated metal slot waveguide on silicon. Opt. Lett. **31**(14), 2133–2135 (2006)

Chu, H., Ewe, W., Koh, W., Li, E.: Remarkable influence of the number of nanowires on plasmonic behaviors of the coupled metallic nanowire chain. Appl. Phys. Lett. **92**(10), 103103 (2008)

Diest, K., Dionne, J.A., Spain, M., Atwater, H.A.: Tunable color filters based on metal–insulator–metal resonators. Nano Lett. **9**(7), 2579–2583 (2009)

Emboras, A., Briggs, R., Najar, A., Nambiar, S., Delacour, C., Grosse, P., Augendre, E., Fedeli, J., De Salvo, B., Atwater, H.: Efficient coupler between silicon photonic and metal–insulator–silicon-metal plasmonic waveguides. Appl. Phys. Lett. **101**(25), 251117 (2012)

Ginzburg, P., Arbel, D., Orenstein, M.: Gap plasmon polariton structure for very efficient microscale-to-nanoscale interfacing. Opt. Lett. **31**(22), 3288–3290 (2006)

Ginzburg, P., Orenstein, M.: Plasmonic transmission lines: from micro to nano scale with $\lambda/4$ impedance matching. Opt. Express **15**(11), 6762–6767 (2007)

Han, Z., Forsberg, E., He, S.: Surface plasmon Bragg gratings formed in metal-insulator-metal waveguides. IEEE Photon. Technol. Lett. **19**(2), 91–93 (2007)

Hodaei, H., Rezaei, M., Miri, M., Bahadori, M., Eshaghian, A., Mehrany, K.: Easy-to-design nano-coupler between metal–insulator–metal plasmonic and dielectric slab waveguides. Plasmonics **8**(2), 1123–1128 (2013)

Kusunoki, F., Yotsuya, T., Takahara, J., Kobayashi, T.: Propagation properties of guided waves in index-guided two-dimensional optical waveguides. Appl. Phys. Lett. **86**(21), 211101 (2005)

Lee, S.-Y., Park, J., Kang, M., Lee, B.: Highly efficient plasmonic interconnector based on the asymmetric junction between metal–dielectric–metal and dielectric slab waveguides. Opt. Express **19**(10), 9562–9574 (2011)

Lima, E.P., Rodriguez-Esquerre, V., Mercedes, C.R., Dourado-Sisnando, A.: Design of dielectric to plasmonic waveguide power transfer couplers. In: Plasmonics: Design, Materials, Fabrication, Characterization, and Applications XV, p. 103462P. International Society for Optics and Photonics (2017)

Liu, L., Han, Z., He, S.: Novel surface plasmon waveguide for high integration. Opt. Express **13**(17), 6645–6650 (2005)

Liu, Y., Lai, Y., Chang, K.: Plasmonic coupler for silicon-based micro-slabs to plasominc nano-gap waveguide mode coversion enhancement. J. Lightwave Technol. **31**(11), 1708–1712 (2013)

Maier, S.A.: Plasmonics: Fundamentals and Applications. Springer, Berlin (2007)

Mei, X., Huang, X., Tao, J., Zhu, J., Zhu, Y., Jin, X.: A wavelength demultiplexing structure based on plasmonic MDM side-coupled cavities. JOSA B **27**(12), 2707–2713 (2010)

Min, C., Veronis, G.: Absorption switches in metal-dielectric-metal plasmonic waveguides. Opt. Express **17**(13), 10757–10766 (2009)

Mote, R.G., Chu, H.-S., Bai, P., Li, E.-P.: Compact and efficient coupler to interface hybrid dielectric-loaded plasmonic waveguide with silicon photonic slab waveguide. Opt. Commun. **285**(18), 3709–3713 (2012)

Pile, D., Gramotnev, D.K.: Adiabatic and nonadiabatic nanofocusing of plasmons by tapered gap plasmon waveguides. Appl. Phys. Lett. **89**(4), 041111 (2006)

Pile, D.F., Ogawa, T., Gramotnev, D.K., Matsuzaki, Y., Vernon, K.C., Yamaguchi, K., Okamoto, T., Haraguchi, M., Fukui, M.: Two-dimensionally localized modes of a nanoscale gap plasmon waveguide. Appl. Phys. Lett. **87**(26), 261114 (2005)

Pozar, D.M.: Microwave engineering. Wiley, New York (2009)

Reiserer, A.A., Huang, J.-S., Hecht, B., Brixner, T.: Subwavelength broadband splitters and switches for femtosecond plasmonic signals. Opt. Express **18**(11), 11810–11820 (2010)

Rezaei, M., Jalaly, S., Miri, M., Khavasi, A., Fard, A.P., Mehrany, K., Rashidian, B.: A distributed circuit model for side-coupled nanoplasmonic structures with metal–insulator–metal arrangement. IEEE J. Sel. Top. Quantum Electron. **18**(6), 1692–1699 (2012)

Tamir, T.: Integrated Optics, Vol. 7 of Topics in Applied Physics. Springer, New York (1975)

Tanaka, K., Tanaka, M.: Simulations of nanometric optical circuits based on surface plasmon polariton gap waveguide. Appl. Phys. Lett. **82**(8), 1158–1160 (2003)

Veronis, G., Fan, S.: Theoretical investigation of compact couplers between dielectric slab waveguides and two-dimensional metal-dielectric-metal plasmonic waveguides. Opt. Express **15**(3), 1211–1221 (2007)

Wahsheh, R.A., Lu, Z., Abushagur, M.A.: Nanoplasmonic couplers and splitters. Opt. Express **17**(21), 19033–19040 (2009)